Auger resonant-Raman decay after Xe *L*-edge photoexcitation

R. K. Kushawaha,[1,2] K. Jänkälä,[3] T. Marchenko,[1,2] G. Goldsztejn,[1,2] R. Guillemin,[1,2] L. Journel,[1,2] D. Céolin,[4] J.-P. Rueff,[1,2,4] A. F. Lago,[5] R. Püttner,[6] M. N. Piancastelli,[1,2,7,*] and M. Simon[1,2,4]

[1]*CNRS, UMR 7614, Laboratoire de Chimie Physique-Matière et Rayonnement, F-75005, Paris, France*

[2]*Sorbonne Universités, UPMC Université Paris 06, UMR 7614, Laboratoire de Chimie Physique-Matière et Rayonnement, 75005 Paris, France*

[3]*Centre for Molecular Materials Research, University of Oulu, Box 3000, 90014 University of Oulu, Finland*

[4]*Synchrotron SOLEIL, l'Orme des Merisiers, Saint-Aubin, Boîte Postale 48, 91192 Gif-sur-Yvette Cedex, France*

[5]*Centro de Ciências Naturais e Humanas, Universidade Federal do ABC (UFABC) Rua Santa Adélia 166, 09210-170, Santo André, São Paulo, Brazil*

[6]*Institut für Experimentalphysik, Freie Universität Berlin, Arnimallee 14, D-14195 Berlin, Germany*

[7]*Department of Physics and Astronomy, Uppsala University, Box 516, 75120 Uppsala, Sweden*

(Received 13 May 2015; published 31 July 2015)

We have investigated resonant Auger decay of xenon following photoexcitation of each of the three L edges under resonant-Raman conditions, which allowed us to characterize several higher Rydberg transitions. Relative intensities for spectator final states reached after L_1-, L_2-, and L_3-edge excitations are studied in detail. Thanks to state-of-the-art experimental arrangements, our results not only reproduce the previously calculated $3d^{-2}5d$ and nd ($n > 5$) state cross sections after L_3 excitation, but also allow extracting the $3d^{-2}6d$ spectator state energy position and revealing its resonant behavior, blurred by the insufficient experimental resolution in previous data sets. The $3d^{-2}6p$ and $3d^{-2}7p$ states reached after L_1 excitation as well as the $3d^{-2}5d$ and $3d^{-2}6d$ states reached after L_2 excitation are also investigated and their relative intensities are reported and compared to *ab initio* Dirac-Hartree-Fock configuration-interaction calculations. We found the signature of electronic-state-lifetime interference effects between several coherently excited intermediate states, due to large lifetime broadening. Electron recapture processes are also identified above all three photoionization thresholds.

DOI: 10.1103/PhysRevA.92.013427 PACS number(s): 32.80.Aa, 32.80.Hd, 31.15.ag

I. INTRODUCTION

Following a photoionization process leading to the creation of a deep core hole in atoms and molecules, the electron vacancy is filled by outer shell-electrons in a complex multistep decay path which can produce multiply ionized species (see, e.g., [1]). The electron ejected in the decay process is known as an Auger electron, and it carries information about the orbital energies and electronic structure of the ionized species. In resonant photoexcitation, when a core electron is promoted to an unoccupied orbital and the hole is filled by another outer electron, the excited electron can act as spectator to or participate in the decay process. These processes are categorized as spectator and participator resonant Auger decay [2,3]. The spectator electron can remain in the initially excited orbital or be shaken up or down to an orbital with a different quantum number [4–6]. The shakeup process was identified in decay from Ar ($1s^{-1}np$) states [7], and spectator transitions were investigated in the decay of $4d$ to np excitation of xenon [4] and in the xenon $L_3M_4M_5$ Auger decay [8,9].

Deep core holes have a short lifetime, and consequently the natural linewidth of the corresponding spectral feature in the absorption spectra is large. If the spacing between core-excited states is of the same order of magnitude as their linewidth, interference between several decay channels involving partially overlapping excited states and leading to the same final states is possible. In the Auger decay following core-to-Rydberg excitations, such electronic-state–lifetime interference can be revealed in the line intensity and profile of the peaks corresponding to the different final states. This phenomenon was predicted in [10], and calculated in the *KLL* spectator Auger decay in argon [11] and in the angular distribution of resonant Auger electrons following Kr $3d$ excitation [12]. It was also verified in Ne, Kr, and HCl in between core-to-Rydberg resonances [13–15]. Experimental evidence for its appearance on top of a resonance after deep core excitation has been recently demonstrated in the Ar *KLL* decay [16].

Traditionally speaking, two regimes can be distinguished while investigating the decay of core-excited states across a resonance: the below- and above-threshold regions. The below-threshold region is characterized by relatively narrow resonant spectral features as the decay channel is indistinguishable from the direct photoionization leading to the same final states of the process. The above-threshold region includes diagram Auger lines which can be distorted and shifted from their asymptotic shape by postcollision interaction (PCI) (see e.g [17,18].) between the escaping photo- and Auger electrons. In the energy region very close to threshold, these two regimes may not be clearly distinguishable anymore, especially for deep-lying core holes which are short lived. In particular, electron recapture effects have to be taken into account, both above and below threshold (see, e.g., [2,19–21]). A recent paper has pointed out the importance of electron recapture in the Auger decay following photoionization of the shallow $4d$ level in Xe [22].

Although few attempts have been made to study the multistep decay processes following deep core excitation (see, e.g., [2,15,21]), energy positions of Rydberg transitions, recapture, and interference effects have not been extensively explored in

*Corresponding author: maria-novella.piancastelli@physics.uu.se

heavy atoms, due to experimental difficulties. The core-hole lifetime of deep-lying levels such as Xe $2s$ and $2p$ is very short (in the few hundreds of attoseconds range), and therefore the corresponding spectral features measured in the energy domain are very broad. Therefore, in order to perform a detailed study of the decay spectra, it is necessary to run experiments under the so-called Auger resonant-Raman conditions [8,23], under which the total experimental resolution should be better than the lifetime broadening. Such experimental conditions for deep edges have become available only recently.

In this work, we report state-of-the-art absorption and Auger decay spectra around the Xe L_1, L_2, and L_3 edges. Previous studies of the Auger decay following Xe excitation and ionization around the L_3 edge have been reported, with limited resolution [8,9]. A more recent work has shown the evolution of the spectator and diagram lines across the threshold, with the aid of radiationless resonant-Raman scattering calculations, and underlined the importance of PCI and recapture effects [2]. However, while the final state $3d^{-2}5d$ was identified, the insufficient experimental resolution available at the time prevented a thorough investigation of the final states of the type $3d^{-2}nd$ with $n > 5$. The present investigation is focused on the spectator cross sections, interference, and recapture effects in photoexcitation of xenon around the L edges. We show that, under Auger resonant-Raman conditions, the photon energy position of transitions to high-lying Rydberg states can be derived from the relative intensities (or pseudopartial cross sections) of the spectator final states; it is not possible to observe this in the absorption curves due to the large lifetime broadening. The high occurrence of shakeup and shakedown processes is also clearly observed in the resonant Auger spectra. Furthermore, from the observation of asymmetric profiles and variations in the widths of the pseudopartial cross sections, the presence of electronic-state–lifetime interference can be assessed. The importance of electron recapture effects is also pointed out.

II. EXPERIMENTAL DETAILS

Recently, the GALAXIES beamline at Synchrotron SOLEIL, Saint Aubin, France, has become operational it is designed to provide a monochromatic focused beam with the highest flux possible in the spectral range of 2.4–13 keV and a photon energy bandwidth between 100 meV and 1 eV [24]. Resonant Auger measurements near L edges of xenon were performed using the hard x-ray photoelectron spectroscopy (HAXPES) end station [25], which allows us to study resonant Auger processes even at deep shells under resonant-Raman condition, i.e., with a total instrumental resolution (including photon bandwidth and electron kinetic energy analyzer) below the core-hole lifetime broadening (see, e.g., [16,26–28] for the performances of the beamline).

With the HAXPES setup, the electron kinetic energy measurements are carried out by the newly designed EW4000 VG-Scienta hemispherical photoelectron analyzer. The instrument is optimized for the detection of electron kinetic energies up to 12 keV with an expected resolution of 35 meV for electrons having a kinetic energy of 10 keV, while providing high transmission thanks to the 60° total horizontal opening angle of the lens. The electron analyzer is mounted on a μ-metal-shielded UHV experimental chamber, and the lens system is placed perpendicularly to the beam and parallel to the electric field vector of the linearly polarized synchrotron light. The gas cell is mounted on a fully motorized four-axis manipulator located at the bottom of the main chamber. A liquid-nitrogen cooling system is integrated with the cell in order to reduce the Doppler broadening contribution. X-ray absorption measurements in the gas phase are performed using the spectrometer in a partial electron yield (PEY) mode. The related electron kinetic energy windows were $3118 - 3618$ eV for L_3, $3438 - 3938$ eV for L_2, and $3783 - 4283$ eV for L_1. The measured resonant Auger spectra as a function of photon energy near L edges are converted to two-dimensional (2D) maps. The resolvable identified spectator Auger decay spectral features at each recorded photon energy are analyzed offline by multipeak Voigt profile fittings and the relative intensities are obtained.A system of differential pumping on both entrance and exit paths of the HAXPES station ensures a high vacuum level in the rest of the beamline even when gas is introduced into the main chamber.

During the measurements on xenon, the pressure in the chamber was maintained at 5×10^{-6} mbar. The analyzer parameters such as pass energy (500 eV) and slit width (400 μm) were fixed during the experiment, yielding a resolution of 0.5 eV. The photon bandwidth was approximately 1 eV at 5 keV photon energy. Since the spectra were recorded at 0° with respect to the linear polarization axis, angular effects, albeit small, could be present and affect the intensity ratios of the different final states. Therefore, in the following we will refer to the relative intensities we measure as "pseudopartial cross sections." Such pseudopartial cross sections were obtained from multipeak Voigt profile fittings of the measured Auger spectra.

The kinetic energy scale was calibrated by using the known energy positions of the Ar *KLL* and Ar *KMM* normal Auger spectra [29,30]. In order to calibrate the photon energy scale, Ar $2p$ photoelectron spectra were obtained in the three-photon energy ranges used for the actual measurements, and calibrated by using the known value of 250.79 eV for the Ar $2p_{1/2}$ binding energy [29].

III. THEORY

The calculations were performed in the relativistic configuration-interaction Dirac-Fock framework, where the atomic state functions (ASFs) are expanded as linear combinations of jj-coupled configuration state functions (CSFs) of the same total angular momentum J and parity P. The coefficients of the linear combination were solved by diagonalizing the Dirac-Coulomb-Breit Hamiltonian in the CSF basis while keeping the radial functions fixed. The one-electron wave functions entering the CSFs were obtained in the average level scheme by applying the GRASP2K package [31] with a modified RSCF component from the GRASP92 program [32]. The ASF mixing coefficients and further relativistic corrections via perturbation theory were solved using the RELCI extension [32].

The configurations included in the calculations of the excited states were $\mathrm{Xe}(2s^{-1})[6p,7p] - \mathrm{Xe}(3d^{-2})[6p,7p]$ and $\mathrm{Xe}(2p^{-1})[5d,6s,6d,7s,7d] - \mathrm{Xe}(3d^{-2})[5d,6s,6d,7s,7d]$.

The ground state and $2s$ and $2p$ ionized states were approximated by single-configuration calculations. The relativistic corrections included transverse Breit interaction, mass shift, and contributions from self-energy and vacuum polarization [33]. In the present case the only considerable relativistic correction (note that for transition energies many corrections tend to cancel out) was the self-energy. The self-energy corrections for the L_1 excited states were about 6.6 eV smaller than for the ground state, which reduced the offset in the excitation energies from about 11.3 to 4.7 eV. For L_2 and L_3 excited states the self-energy corrections were about 0.1 and 0.6 eV smaller than for the ground state, respectively. With this correction the excitation energy difference between experiment and calculation was only about 0.8 eV for the L_2 and 1.0 eV for the L_3 edge.

The resonant Auger decay matrix elements T_{fi} and angle-dependent partial cross sections $\frac{d\sigma_i}{d\Omega} \propto f|T_{fi}|^2$ were calculated following the general resonant scattering formulation by Åberg *et al.* [34]:

$$T_{fi} = \langle \Psi_f | \hat{D} | \Psi_i \rangle + \sum_\beta \int d\tau_\beta \frac{\langle \Psi_f | \hat{H} - E | \Psi_\beta \rangle \langle \Psi_\beta | \hat{D} | \Psi_i \rangle}{E - E_\beta - \tau_\beta + i\Gamma_\beta/2}, \quad (1)$$

where the first term describes the direct photoionization channel and the second the resonant channel. The summation goes over all discrete bound (Rydberg) states and the integration over the continuum states. The formulation is essentially the same as what was used to study similar problems in [20] and [16]. In the present case the first term in (1) is the cross section for direct $3d$ photoionization accompanied by the $3d \rightarrow nl$ shakeup transition, which can be assumed negligibly small at the resonances. In the second term, $\langle \Psi_\beta | \hat{D} | \Psi_i \rangle$ is the dipole photoexcitation matrix element from the initial state i to the intermediate excited or ion+ continuum state β. The element $\langle \Psi_f | \hat{H} - E \langle \Psi_\beta |$ is the Auger decay matrix. In order to account for shake transitions and recapture during the Auger decay, it was assumed that the element is not sensitive to the orbital of the excited spectator electron in state β (except for the formal coupling and overlap), which can be justified by the fact that the decay occurs mainly between deep core orbitals that do not interact considerably with the electron outside the closed $5p$ shell. This allows approximating the element as

$$\begin{aligned} &\langle \Psi_f | \hat{H} - E | \Psi_\beta \rangle \\ &= \langle 3d^{-2}; \epsilon\kappa, n'l_j | \hat{H} - E \big| 2l_j^{-1}, nl_j \big\rangle \\ &\approx \langle 3d^{-2}; \epsilon\kappa, n'l_j | \hat{H} - E \big| 2l_j^{-1}, nl_j \big\rangle \langle n'l_j | nl_j \rangle, \end{aligned} \quad (2)$$

where $|nl_j\rangle$ stands for bound or continuum one-electron orbitals in the intermediate state. The term Γ_β in (1) is the lifetime of state β, which requires calculation of all possible decay channels. Because in the present case only decays to $3d^{-2}nl_j$ final states are of interest, the values were taken from the experiment.

The transition matrix elements (1) and (2) were constructed utilizing the individual programs provided by the RATIP package [33]. The resonant excitation and photoionization matrix elements were obtained using the REOS and PHOTO components, respectively. The continuum wave functions needed for evaluating the recapture probabilities [overlaps in (2)] were calculated using the COWF component of RATIP, extracted to a stand-alone program. The Auger decay matrix elements were calculated using the Auger component modified to account for nonorthogonality of the valence orbitals between the intermediate and final states.

IV. RESULTS AND DISCUSSION

We have measured absorptionlike spectra around the three L edges of Xe in the PEY mode. The spectra have been previously measured with very limited experimental resolution [about 5 eV full width at half maximum (FWHM)] [35,36]. However, due to the large natural linewidth (2.82 eV for Xe $2p_{3/2}$, 3.04 eV for Xe $2p_{1/2}$, and 3.35 eV for Xe $2s$ [37,38]), our spectra show no additional structures. We then measured the Auger electron decay spectra around the three L edges. The resonant Auger spectra were obtained as 2D maps showing the Auger electron kinetic energies as a function of photon energy, using a photon energy step of 100 meV across the resonances, in the kinetic energy region corresponding to the most intense decay channels [2]. This technique allows one to immediately visualize the behavior of the various final states in terms of relative intensities and shifts.

Just below threshold, spectator *LMM* is the dominant decay channel, because deep core L-shell excitation favors spatially close M orbitals in the first decay step. Above threshold, we observe the development of normal Auger spectra, in particular a PCI shift of the diagram lines close to the ionization threshold. The resonant Auger spectra and spectator pseudopartial cross sections for L_1-, L_2-, and L_3-edge excitation and *LMM* Auger decay are discussed in separate sections.

A. Xenon spectator and diagram Auger decay near the L_1 threshold

In Fig. 1 (top) we show the absorption curve around the Xe L_1 edge, and in Fig. 1 (bottom) the 2D map of the corresponding resonant Auger decay.

In Fig. 2 (right panel) we show two experimental and theoretical resonant Auger spectra taken at the photon energy values of the maxima of the $2s \rightarrow 6p$ and $2s \rightarrow 7p$ resonances (5451.37 and 5452.77 eV, respectively). A detailed spectral assignment for the resonant Auger spectra at all three edges will be reported elsewhere [39]. Here we only stress that for both $3d^{-2}6p$ and $3d^{-2}7p$ final states the spectral structures correspond to states labeled $3d^{-2}$ ($^1G_{[4]}$) in *LSJ* coupling. The total angular momentum J is set in parentheses to emphasize the fact that it is not formed in *LSJ* coupling due to the requirement of coupling also the outermost electron to the open core shell. Other couplings are allowed but the related features are too weak to be visible.

We can clearly see a double structure for both resonances, which is mainly due to the large lifetime broadening allowing coherent excitation of several intermediate states. In addition, shake transitions during the resonant Auger decay and final ionic state configuration interaction (FISCI) play a role. In shakeup transitions the spectator $6p$ electron can be promoted to the $7p$ orbital, due to orbital relaxation, and the spectator $7p$ electron can end up in the $6p$ orbital due

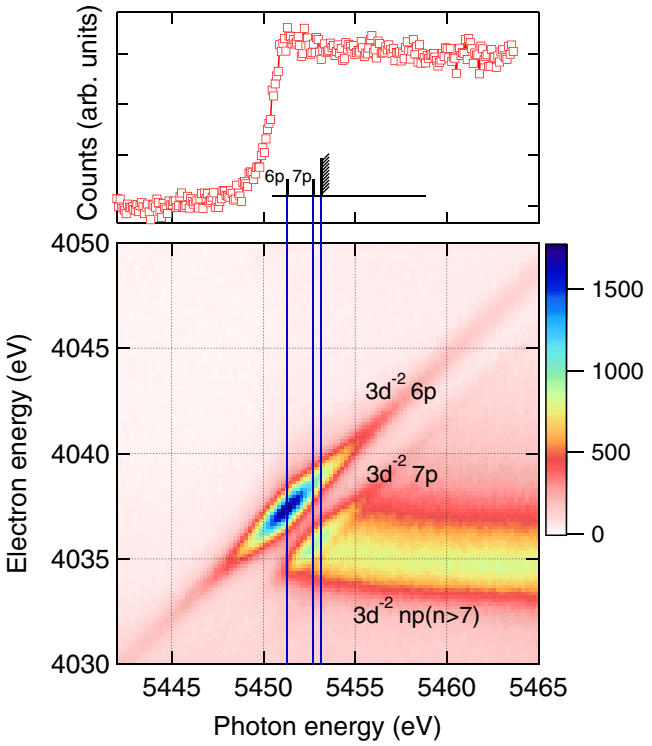

FIG. 1. (Color online) Top: absorption curve around the L_1 edge; bottom: 2D map of the corresponding resonant Auger decay.

to a shakedown. According to our calculations, $3d^{-2}6p$ and $3d^{-2}7p$ configurations mix considerably (states characterized by $3d^{-2}6p$ CSFs have about 10% $3d^{-2}7p$ CSF contribution), which leads to probability for $2s^{-1}6p \rightarrow 3d^{-2}7p$ Auger decay via FISCI. We are unable to resolve np states with $n > 7$. Note that these states are also populated especially in $2s \rightarrow 7p$ excitation, which is the main reason for asymmetry at the low-kinetic-energy side as well as for the higher intensity observed for the $3d^{-2}7p$ peak in the experiment in comparison to the calculations that omit $2s \rightarrow np$ $(n > 7)$ excitations.

The $3d^{-2}6p$ and $3d^{-2}7p$ spectator Auger experimental pseudopartial cross sections and the theoretical results are shown in Fig. 2 (left panel). We can deduce from their intensity distribution that the Xe $2s \rightarrow 6p$ excitation process is the main channel, in agreement with [33]. In addition to the $2s \rightarrow 6p$ excitation, we are able to identify the final state $3d^{-2}7p$, and to derive its pseudopartial cross section. Some higher $np(n > 6)$ states also are populated, but their intensities are rather low. As the excitation energy approaches threshold, the energy spacing between excited levels decreases so much that individual resonances are no longer visible.

We notice that the shape of the profiles for the $3d^{-2}6p$ and $3d^{-2}7p$ states' pseudopartial cross sections is asymmetric (more so for the $3d^{-2}7p$ state). Furthermore, the width of the feature corresponding to the $3d^{-2}7p$ state is considerably narrower than the lifetime broadening of the L_1 hole state. The obtained values are 3.57 eV for the $3d^{-2}6p$ state and 1.56 eV for the $3d^{-2}7p$, to compare with the "expected" lifetime broadening of 3.35 eV [37,38]. We attribute these findings to electronic-state–lifetime interference (see more detailed discussion below). This experimental finding is also reproduced by the calculations.

We also observe that there is some intensity for both the $3d^{-2}6p$ and the $3d^{-2}7p$ states above the ionization threshold, in particular for the $3d^{-2}7p$ state which even shows an additional hump around 5456 eV. This is a clear evidence for recapture processes taking place. The recapture processes can also affect the pseudopartial cross section below threshold, as reported in [2,20,21].

B. Xenon spectator and diagram Auger decay near the L_2 threshold

The absorption curve around the Xe L_2 edge and the related 2D map for the electron decay are shown in Fig. 3 top and bottom, respectively. Near the L_2 and L_3 thresholds, the $2p$ electron is excited to $nd(n = 5,6,\ldots)$ orbitals and remains as a spectator while $3d$ electrons participate in the Auger decay. As for the L_1 edge, excited high Rydberg states heavily overlap,

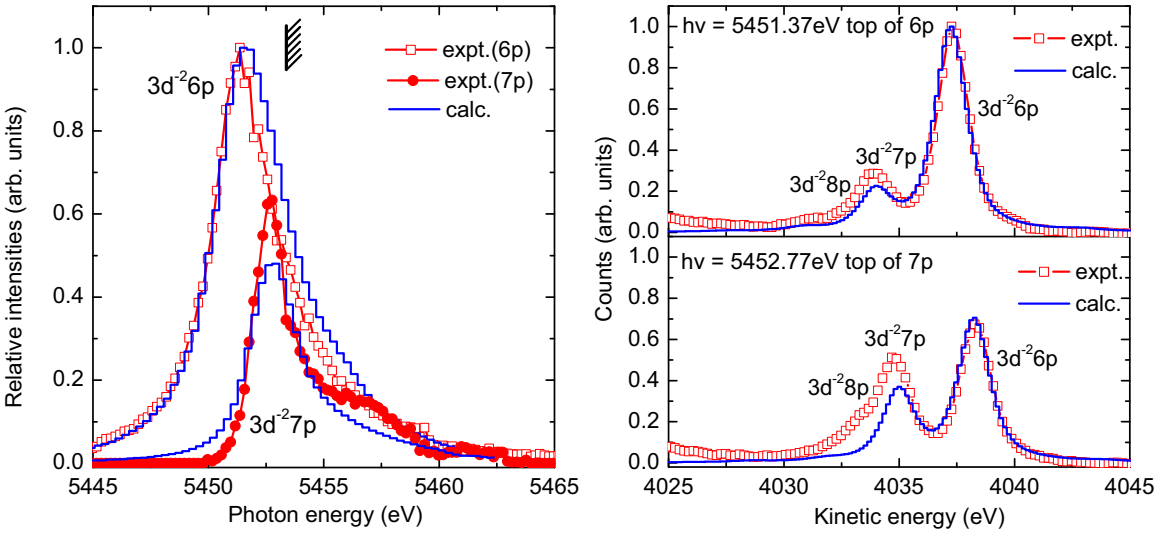

FIG. 2. (Color online) Left: pseudopartial cross sections for the $3d^{-2}6p$ and $3d^{-2}7p$ final states reached after resonant Auger decay at the L_1 edge. Right: resonant Auger spectra following excitations below the L_1 edge.

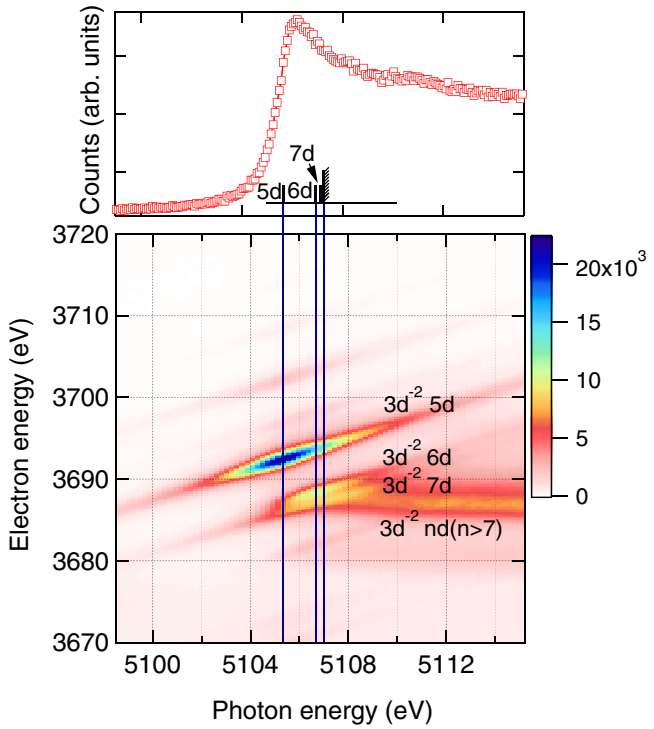

FIG. 3. (Color online) Top: absorption curve around the L_2 edge; bottom: 2D map of the corresponding resonant Auger decay.

so that $3d^{-2}7d$ is the highest final state that can be identified (but not individually resolved) in the 2D map.

The dominant photoexcitation processes lead to the population of nd Rydberg states. In [35] transitions to ns Rydberg states are also taken into account, but shown to be very weak. Therefore we assume that in our decay spectra all final states are of $3d^{-2}nd$ configuration. The assumption is also confirmed by the present calculations which give about 15 times larger oscillator strengths for $2p \rightarrow nd$ than for $2p \rightarrow ns$ excitations. The resonant Auger spectra taken at 5105.4 eV (on top of the $2p \rightarrow 5d$ transition) and 5106.6 eV (on top of the $2p \rightarrow 6d$ transition) and the $3d^{-2}5d$ and $3d^{-2}6d$ pseudopartial cross sections are shown in the right and left panels of Fig. 4, respectively.

The $3d^{-2}5d$ and $3d^{-2}6d$ final states are resolved in the below-threshold spectra, although there is a substantial overlap with higher state(s). Both these final states are labeled $3d^{-2}$ ($^1G_{[4]}$) in LSJ coupling. Some weaker features can also be assigned, such as the peaks at 3698.5 eV, 3682.5, eV and 3681 eV kinetic energy in the top curve of Fig. 4 (right panel), corresponding respectively to $3d^{-2}$ ($^3P_{[0,1,2]}$)$5d$, $3d^{-2}$ ($^1D_{[2]} + {}^3F_{[2]}$)$6d$, and $3d^{-2}$($^1D_{[2]} + {}^3F_{[2]}$)$[7d + nd]$ states. A more detailed discussion on all structures will be reported elsewhere [39]. Here we concentrate on the prominent features.

The FWHMs of Auger pseudopartial cross sections are 4.42 eV for the $3d^{-2}5d$ and 3.76 eV for the $3d^{-2}6d$ states (Fig. 4, left), to compare with a lifetime width of 3.04 eV [37,38]. Their line shape is asymmetric. Again, we attribute such asymmetry to electronic-state–lifetime interference. In analogy with the L_1 threshold, we observe electron recapture processes well above the ionization threshold.

C. Xenon spectator and diagram Auger decay near the L_3 threshold

The absorption curve around the Xe L_3 edge and the related 2D map for the electron decay are shown in Fig. 5, top and bottom. The resonant Auger spectra at 4784.89 eV (on top of the $2p \rightarrow 5d$ transition) and at 4787.09 eV (on top of the $2p \rightarrow 6d$ transition) and the $3d^{-2}5d$ and $3d^{-2}6d$ Auger pseudopartial cross sections are shown in the right and left panels of Fig. 6, respectively.

As for the spectral assignment, the situation is completely analogous to that of the L_2 edge: the most prominent spectral features are related to states labeled $3d^{-2}$ ($^1G_{[4]}$) in LSJ coupling. This is consistent with previous measurements [2,8,9].

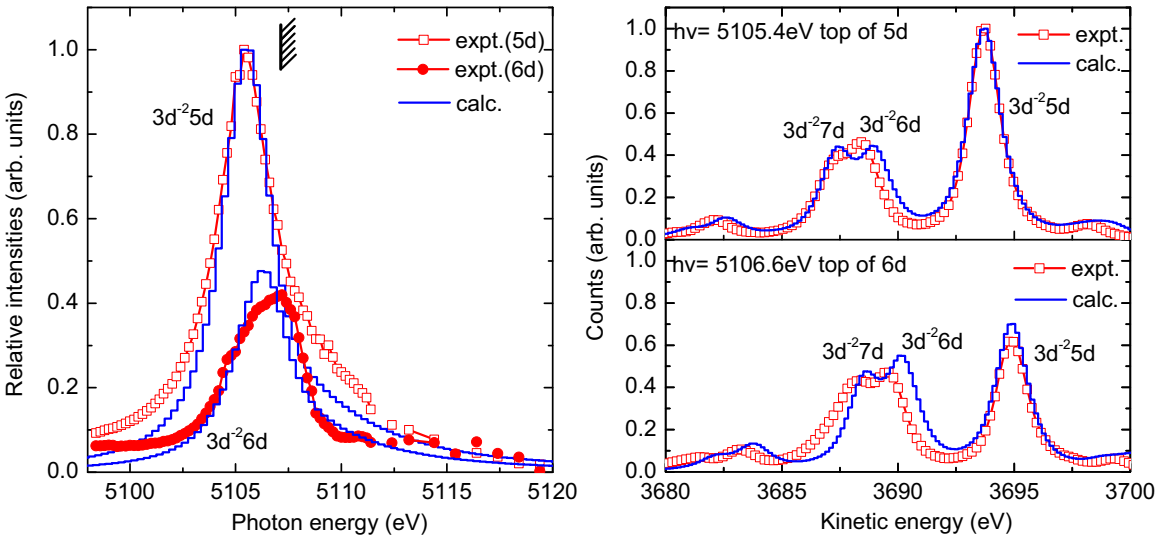

FIG. 4. (Color online) Left: pseudopartial cross sections for the $3d^{-2}5d$ and $3d^{-2}6d$ final states reached after resonant Auger decay at the L_2 edge; right: resonant Auger spectra following excitations below the L_2 edge.

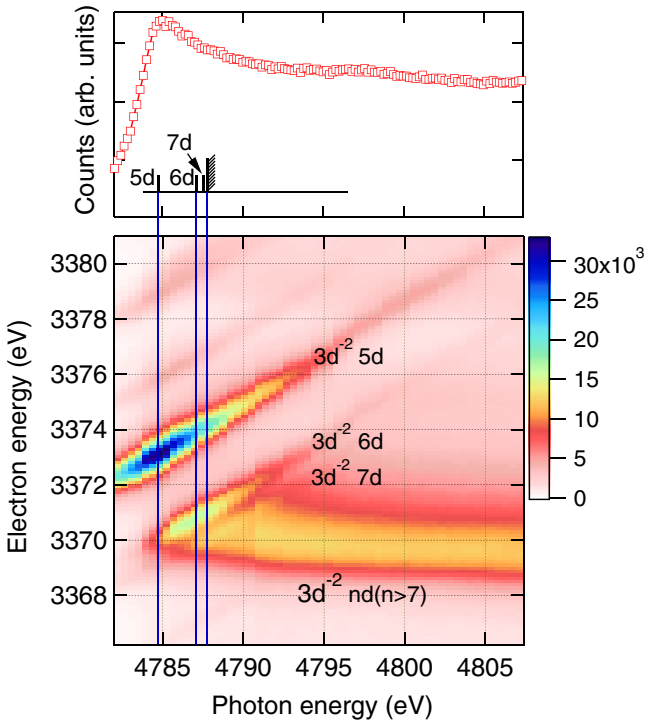

FIG. 5. (Color online) Top: absorption curve around the L_3 edge; bottom: 2D map of the corresponding resonant Auger decay.

The $3d^{-2}5d$ and $3d^{-2}6d$ spectator cross sections are asymmetric, which is again the signature of contribution from more than one excited intermediate state. The unique profile of $3d^{-2}6d$ is due to an interference effect, as confirmed by calculations (see the discussion below). Furthermore, the FWHMs for the $3d^{-2}5d$ and $3d^{-2}6d$ pseudopartial cross sections obtained by Voigt fitting are 2.85 and 1.73 eV, respectively, to compare with a lifetime broadening of 2.82 eV [37,38].

Although the possibility of interference was mentioned in [2], the corresponding experimental observation was hindered up to now due to the relatively poor experimental resolution previously available (1.5 eV photon bandpass and 1.1 eV spectrometer resolution) [2].

In analogy with the L_1 and L_2 thresholds, we observe electron recapture processes well above the ionization threshold.

D. Discussion

The Auger resonant-Raman conditions under which we were able to measure Auger decay spectra allow us to shed additional light on the dynamics of photoabsorption and relaxation processes at the Xe L edges. The large lifetime broadening hinders the measurement of better-resolved absorption spectra despite the improved experimental performances. However, we are able to identify the position and photon energy dependence of several Rydberg states which are not clearly visible in the absorption curves.

At the L_1 threshold, the width of the pseudopartial cross section for the $3d^{-2}7p$ state is considerably narrower, whereas the $3d^{-2}6p$ state is somewhat broader than the expected core-hole lifetime broadening. Such variations in the line profile are reproduced by the calculations, which take into account the coherent excitation to the $6p$ and $7p$ Rydberg states and therefore the electronic-state–lifetime interference. Because of the large lifetime broadening, a coherent excitation of more than one intermediate state is possible, which causes interference between decay channels when the same final states are reached. In the present case, this phenomenon manifests itself via destructive interference in the line profile of pseudopartial cross sections of the final states. Similar effects have been theoretically predicted [11] and experimentally demonstrated [16] for argon.

Similar findings are reported for the L_2 and L_3 edges, where strong shakeup and shakedown processes are evidenced. Distorted shapes in the pseudopartial cross sections are also observed. Furthermore, the FWHM of the pseudopartial cross section of the $3d^{-2}6d$ final state reached after L_3 excitation is much narrower than the lifetime broadening. Once again, these findings reveal electronic-state–lifetime interference phenomena due to coherent excitation of more than one intermediate state. Interestingly, the measurements show clear differences between the pseudopartial cross sections for the $3d^{-2}6d$ final state after $2p_{1/2} \rightarrow 6d$ and $2p_{3/2} \rightarrow 6d$ absorption processes. The one after $2p_{3/2} \rightarrow 6d$ excitation (Fig. 6, left) is narrow and similar to the $2s \rightarrow 7p$ case (Fig. 2, left), whereas the one after $2p_{1/2} \rightarrow 6d$ (Fig. 4, left) is broad, which indicates overlapping unresolved contributions from shake processes.

We notice that the $3d^{-2}nl$ final states, created from resonant Auger decay, show a long tail and some structures above the ionization threshold, where states with two vacancies reached by normal Auger decay are also present. Such features are a clear indication of electron recapture, which for resonant Auger states can be considered as shakedown processes from continuum states. The physical picture is the following [20,21]: above threshold, a photoelectron is ejected and starts moving away from the ion core. Later on, the Auger decay of the core kicks in, and the fast Auger electron overtakes the slow photoelectron. The photoelectron experiences an increase in the ionic central potential and loses energy, while the Auger electron accelerates (see, e.g., [40] for recent results). This is the usual description of PCI energy shift of photoelectron and diagram Auger lines near threshold.

At energies near the ionization threshold, the photoelectron energy loss becomes large enough that the initially free photoelectron can be recaptured by the ion into one of the Rydberg states. Therefore, spectator resonant Auger states are populated at the expense of normal Auger states near threshold. In our data set, the signature of recapture is the enhancement of the pseudopartial cross sections of the resonant Auger final states above ionization threshold.

The phenomenon is also qualitatively predicted by the present theoretical modeling based on the monopole approximation. The recapture probability appears to be slightly overestimated for the L_1 edge and underestimated for L_2 and L_3. One clear reason for the disagreement is that below threshold contributions from high Rydberg excitations are missing from the theoretical treatment. Also, in order to draw a complete picture of the recapture process, one needs to explicitly account for electron-electron interaction between the two outgoing electrons.

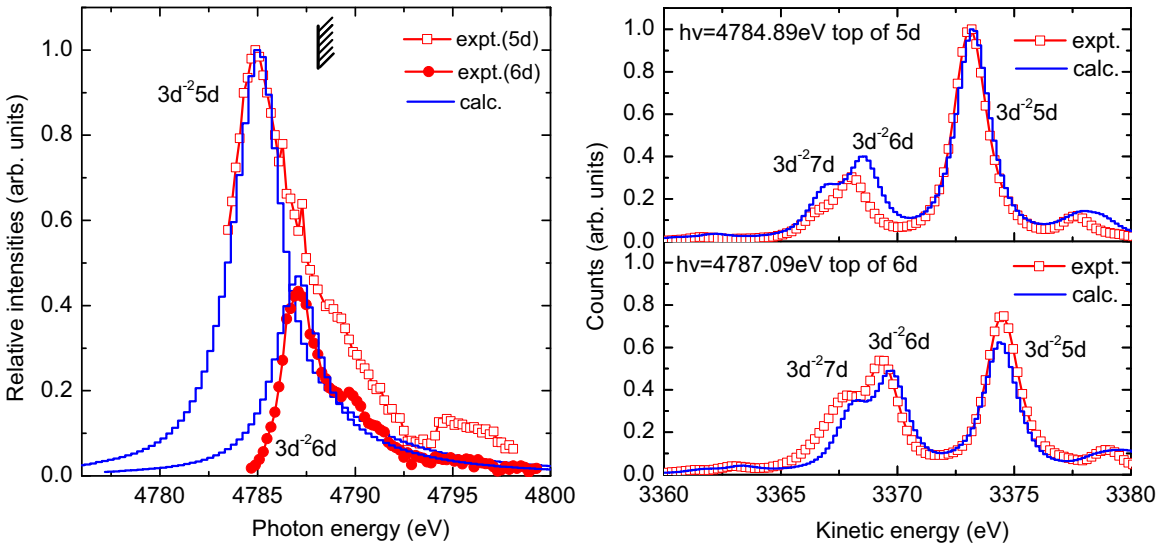

FIG. 6. (Color online) Left: pseudopartial cross sections for the $3d^{-2}5d$ and $3d^{-2}6d$ final states reached after resonant Auger decay at the L_3 edge, right: resonant Auger spectra following excitations below the L_3 edge.

We also notice that the agreement between experimental and theoretical pseudopartial cross section curves is very good for the L_1 threshold, and less so for the other two thresholds. In particular, theory is able to reproduce the asymmetry, but fails in describing fine details. In particular, the irregular shape of the $3d^{-2}6d$ final-state pseudopartial cross section at both L_2 and L_3 excitations is only qualitatively reproduced. We attribute the discrepancy to two limitations. The first is that the calculations underestimate the electron recapture, which is clearly evident on the high-energy side of both curves. The second limitation is that $3d^{-2}nd$ states, with $n \geqslant 7$, overlap with $3d^{-2}6d$, and in the experiment it is rather hard to separate the various contributions.

V. CONCLUSION

We have investigated spectator and diagram Auger decay in xenon near the L_1, L_2, and L_3 thresholds under resonant-Raman experimental conditions. In the case of L_1 photoionization, we have been able to resolve the $3d^{-2}6p$ and the $3d^{-2}7p$ spectator final states which are not distinguishable in absorption measurements. We were also able to resolve the $3d^{-2}5d$ and $3d^{-2}6d$ spectator Auger final states near the L_2 and L_3 edges. The signature of electronic- state–lifetime interference is clearly observed in the pseudopartial cross-section profiles and their widths. Evidence for electron recapture above threshold is also shown.

ACKNOWLEDGMENTS

The authors would like to thank the SOLEIL synchrotron staff for the smooth operation of the facility and the personnel of the GALAXIES beamline for assistance in setting up the experiment. M.N.P. and R.K.K. wish to thank the ANR (Agence Nationale de la Recherche) for financial support in the framework of a “Chaire d Excellence” grant. A.F.L. acknowledges CAPES (Coordenação de Aperfeiçoamento de Pessoal de Nível Superior), Brazil for financial support.

[1] R. Guillemin, C. Bomme, T. Marin, L. Journel, T. Marchenko, R. K. Kushawaha, N. Trcera, M. N. Piancastelli, and M. Simon, Phys. Rev. A **84**, 063425 (2011).
[2] G. B. Armen, S. H. Southworth, J. C. Levin, U. Arp, T. LeBrun, and M. A. MacDonald, Phys. Rev. A **56**, R1079 (1997).
[3] A. G. Kochur and V. L. Sukhorukov, J. Phys. B **29**, 3587 (1996).
[4] U. Becker, D. Szostak, M. Kupsch, H. G. Kerkhoff, B. Langer, and R. Wehlitz, J. Phys. B **22**, 749 (1989).
[5] G. B. Armen, J. Phys. B **29**, 677 (1996).
[6] B. Langer, N. Berrah, A. Farhat, O. Hemmers, and J. D. Bozek, Phys. Rev. A **53**, R1946 (1996).
[7] T. LeBrun, S. H. Southworth, G. B. Armen, M. A. MacDonald, and Y. Azuma, Phys. Rev. A **60**, 4667 (1999).
[8] G. S. Brown, M. H. Chen, B. Crasemann, and G. E. Ice, Phys. Rev. Lett. **45**, 1937 (1980).
[9] G. B. Armen, T. Åberg, J. C. Levin, B. Crasemann, M. H. Chen, G. E. Ice, and G. S. Brown, Phys. Rev. Lett. **54**, 1142 (1985).
[10] A. Cesar and H. Ågren, Phys. Rev. A **45**, 2833 (1992).
[11] G. B. Armen, J. C. Levin, and I. A. Sellin, Phys. Rev. A **53**, 772 (1996).
[12] S Heinäsmäki, K Jänkälä, and J Niskanen, J. Phys. B **42**, 085002 (2009).
[13] J.-E. Rubensson, M. NeebI, A. Bringer, M. Biermann, and W. Eberhardt, Chem. Phys. Lett. **257**, 447 (1996).
[14] E. Kukk, H. Aksela, A. Kivimäki, J. Jauhiainen, E. Nõmmiste, and S. Aksela, Phys. Rev. A **56**, 1481 (1997).
[15] M. Kavčic, M. Žitnik, K. Bučar, A. Mihelič, S. Carniato, L. Journel, R. Guillemin, and M. Simon, Phys. Rev. Lett. **105**, 113004 (2010).

[16] D. Céolin, T. Marchenko, R. Guillemin, L. Journel, R. K. Kushawaha, S. Carniato, S.-M Huttula, J.-P. Rueff, G. B. Armen, M. N. Piancastelli, and M. Simon, Phys. Rev. A **91**, 022502 (2015).
[17] M. Yu. Kuchiev and S. A. Sheinerman, Sov. Phys. Usp. **32**, 569 (1989).
[18] V. Schmidt, Rep. Prog. Phys. **55**, 1483 (1992).
[19] J. Tulkki, T. Åberg, S. B. Whitfield, and B. Crasemann, Phys. Rev. A **41**, 181 (1990).
[20] G. B. Armen, H. Aksela, T. Åberg, and S. Aksela, J. Phys. B **33**, R49 (2000).
[21] R. Guillemin *et al.* (unpublished).
[22] S. Kosugi, M. Iizawa, Y. Kawarai, Y. Kuriyama, A. L. D. Kilcoyne, F. Koike, N. Kuze, D. S. Slaughter, and Y. Azuma, J. Phys. B **48**, 115003 (2015).
[23] A. Kivimäki, A. Naves de Brito, S. Aksela, H. Aksela, O.-P. Sairanen, A. Ausmees, S. J. Osborne, L. B. Dantas, and S. Svensson, Phys. Rev. Lett. **71**, 4307 (1993).
[24] J.-P. Rueff, J. M. Ablett, D. Céolin, D. Prieur, T. Moreno, V. Balédent, B. Lassalle-Kaiser, J. E. Rault, M. Simon, and A. Shukla, J. Synch. Rad. **22**, 175 (2015).
[25] D. Céolin, J. M. Ablett, D. Prieur, T. Moreno, J.-P. Rueff, T. Marchenko, L. Journel, R. Guillemin, B. Pilette, T. Marin, and M. Simon, J. Electron Spectrosc. Relat. Phenom. **190**, 188 (2013).
[26] M. Simon, R. Püttner, T. Marchenko, R. Guillemin, R. K. Kushawaha, L. Journel, G. Goldsztejn, M. N. Piancastelli, J. M. Ablett, J.-P. Rueff, and D. Céolin, Nat. Commun. **5**, 4069 (2014).
[27] M. N. Piancastelli, G. Goldsztejn, T. Marchenko, R. Guillemin, R. K. Kushawaha, L. Journel, S. Carniato, J.-P. Rueff, D. Céolin, and M. Simon, J. Phys. B **47**, 124031 (2014).
[28] R. Püttner, G. Goldsztejn, D. Céolin, J.-P. Rueff, T. Moreno, R. K. Kushawaha, T. Marchenko, R. Guillemin, L. Journel, D. W. Lindle, M. N. Piancastelli, and M. Simon, Phys. Rev. Lett. **114**, 093001 (2015).
[29] L. Avaldi, G. Dawber, R Camilloni, G. C. King, M. Rope, M. R. F. Siggels, G. Stefani, and M. Zitnik, J. Phys. B **27**, 3953 (1994).
[30] M. Breinig, M. H. Chen, G. E. Ice, F. Parente, B. Crasemann, and G. S. Brown, Phys. Rev. A **22**, 520 (1980).
[31] P. Jönsson, X. He, C. Froese Fischer, and I. P. Grant, Comput. Phys. Commun. **177**, 597 (2007).
[32] F. A. Parpia, C. Froese Fischer, and I. P. Grant, Comput. Phys. Commun. **94**, 249 (1996).
[33] S. Fritzsche, C. Froese Fischer, and G. Gaigalas, Comput. Phys. Commun. **148**, 103 (2002).
[34] T. Åberg, Phys. Scr., **T41**, 71 (1992).
[35] F. Wuillemier, Phys. Rev. A **6**, 2067 (1972)
[36] T. Koizumi, T. Hayaishi, T. Matsuo, K. Shima, H. Tawara, T. Tonuma, and A. Yagishita, J. Phys. Soc. Jpn. **58**, 13 (1989).
[37] M. H. Chen, B. Crasemann, and H. Mark, Phys. Rev. A **24**, 177 (1981).
[38] J. L. Campbell and T. Papp, At. Data Nucl. Data Tables **77**, 1 (2001).
[39] M. N. Piancastelli *et al.* (unpublished).
[40] R. Guillemin, S. Sheinerman, C. Bomme, L. Journel, T. Marin, T. Marchenko, R. K. Kushawaha, N. Trcera, M. N. Piancastelli, and M. Simon, Phys. Rev. Lett. **109**, 013001 (2012).